AIAA JOURNAL
Vol. 30, No. 11, November 1992

Analytical Solutions for Hypersonic Flow Past Slender Power-Law Bodies at Small Angle of Attack

A. Merlen* and D. Andriamanalina†
Office National d'Etudes et de Recherches Aérospatiales, 59000 Lille, France

Hypersonic flows around axisymmetrical power-law slender bodies are calculated for high, but finite, Mach numbers and for low angles of attack. This is done by a small perturbation expansion of self-similar solutions using the equivalence principle. The solutions depend only on the exponent n of the power law defining the body and on the specific heat ratio γ of the gas, which is assumed to be perfect and inviscid. These solutions, the shock equation, the pressure coefficient on the body, and the aerodynamic coefficients are obtained in universal analytical form and depend on numerical coefficients determined once and for all for each pair (η,γ). The effects of the angle of attack for nonconical noses is an innovation presented here: we observe that the effect of γ on the shift of the shock and on the normal force and pitching coefficients depends, both in its sense and its intensity, on the shape of the nose cone. Finally, the stream functions are found to generalize Hayes' and Probstein's entropy correction principle to these three-dimensional flows. The results tabulated in this paper are intended to be used as test cases for inviscid numerical simulation and comparisons with specific experiments.

Nomenclature

$C_p, C_x, C_z, C_{mx}, C_m$	= aerodynamic coefficients defined by Eqs. (41), (46), (53), (51), and (55), respectively
F_x, F_z	= aerodynamic force components on the obstacle
M	= Mach number
n	= exponent of the law defining the variation of R and R' as a function of x
O_L	= center of the maximum cross section (Fig. 1)
p, ρ, c	= pressure, density, and speed of sound, respectively
R	= shock position
R'	= position of body surface
r, θ	= polar coordinates in a plane x = const (Fig. 1)
S_{ref}	= reference area defined by Eq. (45)
u, v	= radial and orthoradial components of the velocity, respectively
V_∞	= freestream velocity
w	= x component of the perturbation velocity
x, y, z	= Cartesian coordinates in the physical frame of reference, in which x lies along the axis of symmetry of the obstacle
α	= angle of attack
γ	= specific heat ratio
ζ	= variable defined by Eq. (22) expressing the effects of p_∞
η	= variable defined by Eq. (22) expressing the effect of α
ξ	= dimensionless variable defined by Eq. (23)
$\xi_0, \xi_1, \xi_2, \xi'_0$	= dimensionless numbers defined by Eq. (23)
Σ	= geometric surface of the shock
Σ'	= geometric surface of the obstacle
σ, ψ	= angles defined in Fig. 1
τ	= relative thickness of the body
Φ	= stream function defined by Eq. (65)
Φ_1	= function defined by Eq. (66)
Ψ	= stream function defined by Eq. (63)

Subscripts

c	= values on the downstream face of the shock
i	= values on the point where a given streamline cuts through the shock
x, ξ	= derivative of a function with respect to x and ξ
0	= dimensionless quantities for the self-similar problem
1	= dimensionless quantities for the incidence problem
2	= dimensionless quantities of the p_∞ problem
∞	= freestream quantities

Superscripts

$\tilde{f}$	= values of f with entropy correction
$'$	= values of the body surface
*	= tabulated values

I. Introduction

DURING the years from 1955 to 1965, analytical theories have had a great success in hypersonic aerodynamics. Because of the spectacular development of computational techniques, these theories have lost their role as calculation methods, although they are still useful references for physical understanding and preliminary analysis.

Consequently, methodological questions rise today within the aeronautical community. Do the "classical" methods of theoretical aerodynamics survive in front of the success of computational fluid dynamics? Do we definitively have to give up obtaining analytical relations and use the "numerical wind tunnel" without questions? What will the cultural background of aerodynamics be made of in the future?

Opinions diverge on the subject. To shed some light on the dispute, we decided to compare the results of the theoretical, experimental, and numerical approaches in a case of three-dimensional hypersonic flow. This paper presents the theoretical part of this research.

There are few examples of analytical solutions to three-dimensional hypersonic flows, even for an inviscid perfect gas in an adiabatic flow. The only case that has been gone into in any depth, though, is that of the circular cone. Cheng[1] solved this problem with the Newtonian approximation, and Doty and Rasmussen[2] found constant-density solutions.

The reader will find here analytical solutions for a more extensive class of simple bodies, i.e., axisymmetric power-law

Received July 22, 1991; revision received April 7, 1992; accepted for publication April 7, 1992.

*Consultant, Institut de Mécanique des Fluides, Doctor d'Etat Ingeneieur civil de L'Aéronautique, Université des sciences et techniques de Lille (UFR Mathématique, dept. Mécanique).

†Doctor in Mechanics, Institut de Mécanique des Fluides, Laboratoire de Mécanique de Lille, (URA-CNRS), Université des sciences et techniques de Lille.

bodies. Chernyi,[3] Mirels,[4] and Guiraud[5] discussed at length the axisymmetric flow around these bodies in the framework of the equivalence principle for an infinite Mach number. Kubota[6] extended the results of finite Mach numbers by introducing a perturbation in the basic solution. Lees[7] and Yasuhara[8] discussed the viscous correction. But only Mirels[4] produced a rough modeling of the flow with a nose cone at incidence, in the form of a perturbation of the shock shape and the nose cone. No further work seems to have been done on this modeling.

We should also recall the works of Mirels[4] and Guiraud[5] on the physical validity of solutions stemming from the equivalence principle for power-law bodies. These theoretical results can be summed up roughly by considering that the equivalence principle yields good results for pressures on the obstacle if the power-law exponent n is given a value between ⅔ and 1. The experiments of Kubota[6] confirm these values. Hayes and Probstein[9] emphasized the poor description it provides of the blunting and of the consequences the blunting has on the density at the body surface. However, they do show that, if the stream function is known, the entropy really acquired at the passage through the shock can be reassigned to each streamline to correct the density thusly. To extend this principle to the three-dimensional flow discussed here, the two stream functions of the flow had to be determined analytically. These, as well as the universal functions giving the local properties within the flow, are given for the first time in tabular form in the present paper, for three (n,γ) pairs.

All of these results apply to sufficiently slender bodies. The experimental findings of Kubota[6] and the second-order small perturbation calculations of Townsend[10] show that the condition $R_x^2 \ll 1$ is sufficient. On the other hand, by broadening the range of bodies treated, the present theory loses one degree of freedom with respect to that of Doty and Rasmussen, whose theory can apply for any value of $M_\infty\tau$ because, for the cone, the conditions on the shock only depend on the cone angle. Here, the decoupling of the M_∞ and α effects requires that $M_\infty^2\tau^2 \gg 1$.

II. Formulation

The gas is assumed to be inviscid and thermodynamically perfect, having the specific heat ratio γ. The equation of the body Σ' is

$$R' = \frac{\tau L}{2}\left(\frac{x}{L}\right)^n \tag{1}$$

In a hypersonic configuration, the flow is contained in a thin layer between the shock and the body, and if $(\gamma-1)$ is assumed to be of the order of unity, it is natural to assume that the physical quantities in this layer are of the order of their value ahead of the shock. Except for the blunted area, which is very small if $1 \geq n \geq ⅔$, the angle σ formed by the tangent to the shock in the plane (V_∞, V_c) and the direction of V_∞ verifies the following hypotheses:

$$\begin{gathered} \sin^2\sigma \ll 1 \\ M_\infty^2 \sin^2\sigma \gg 1 \end{gathered} \tag{2}$$

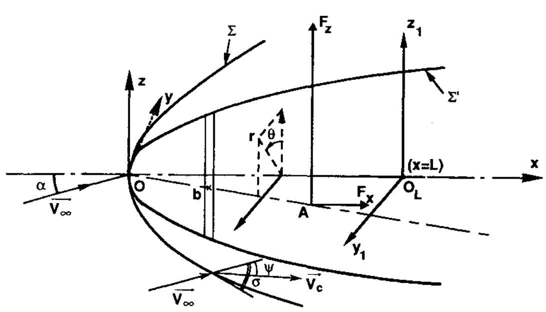

Fig. 1 Notations.

The equation of the shock Σ is $r = R(x,\theta)$. Using the hypotheses (2) and assuming a low angle of attack defined by

$$|\alpha| \ll 1 \tag{3}$$

the conditions across the shock can be written in the linearized form:

$$\frac{\rho_\infty}{\rho_c} = \frac{\gamma-1}{\gamma+1}\left(1+\frac{2}{\gamma-1}\frac{1}{M_\infty^2\sin^2\sigma}\right) \tag{4}$$

$$p_c = \frac{2\rho_\infty V_\infty^2 \sin^2\sigma}{\gamma+1}\left(1-\frac{\gamma-1}{2\gamma}\frac{1}{M_\infty^2\sin^2\sigma}\right) \tag{5}$$

$$V_c = V_\infty\,[1+0(\sigma^2,\alpha^2)] \tag{6}$$

$$\psi_c = \frac{2\sigma}{\gamma+1}\left(1-\frac{1}{M_\infty^2\sin^2\sigma}\right)[1+0(\sigma^2)] \tag{7}$$

in which ψ_c is the angle $\langle V_\infty, V_c\rangle$. So we can easily give the order of magnitude of the unknowns:

$$\rho \sim \rho_c \sim \rho_\infty \tag{8}$$

$$p \sim p_c \sim \rho_\infty V_\infty^2 \sigma^2 \tag{9}$$

$$\sqrt{u^2+v^2} \sim \sqrt{u_c^2+v_c^2} \sim V_\infty\sigma \tag{10}$$

$$w \sim w_c \sim V_\infty\sigma^2 \tag{11}$$

where we have let $V = (V_\infty + w, u, v)$. With these orders of magnitude, we know[3,6,10,11] that the system of equations can be put in degenerate form:

$$V_\infty\rho_x + \frac{1}{r}(r\rho u)_r + \frac{1}{r}(\rho v)_\theta = 0 \tag{12}$$

$$V_\infty u_x + uu_r + \frac{v}{r}u_\theta - \frac{v^2}{r} + \frac{1}{\rho}p_r = 0 \tag{13}$$

$$V_\infty v_x + uv_r + \frac{v}{r}v_\theta + \frac{uv}{r} + \frac{1}{\rho r}p_\theta = 0 \tag{14}$$

$$V_\infty\left(\frac{p}{\rho^\gamma}\right)_x + u\left(\frac{p}{\rho^\gamma}\right)_r + \frac{v}{r}\left(\frac{p}{\rho^\gamma}\right)_\theta = 0 \tag{15}$$

with one further decoupled equation for the longitudinal perturbation velocity:

$$w = -\frac{c^2}{(\gamma-1)V_\infty} - \frac{u^2+v^2}{2V_\infty} \tag{16}$$

By calculating $\sin\sigma$ as a function of R and of the angle of attack α, we have more generally

$$\sin\sigma = \frac{R_x\cos\alpha}{\sqrt{1+R_x^2+m^2}}\left[1-\frac{\tan\alpha}{R_x}(\cos\theta - m\sin\theta)\right] \tag{17}$$

in which $R_x = (\partial R/\partial x)$ and $m = (1/R)(\partial R/\partial\theta)$. With hypotheses (2) and (3) and neglecting α^2-order terms, the most general form of R is $R = R^0(x) + \alpha R^1(x,\theta) + 0(\alpha^2)$. The function R^1 necessarily depends on x, or else R_x would be independent of α. For shocks sufficiently regular in shape, if hypothesis (3) is verified, Eq. (17) reduces to

$$\sin\sigma = \frac{R_x}{\sqrt{1+R_x^2}}\left(1-\frac{\alpha}{R_x^0}\cos\theta\right) \tag{18}$$

So it can be seen that, independent of the value of R_x^0, the condition (3) reveals the effect of α in the form of an expansion in the variable α/R_x^0. If R_x^0 is of order one or higher, the terms in α/R_x^0 become negligible for the same reason as the terms in α. For this reason, only that part of the shock corresponding to the slender body hypothesis is sensitive to the incidence effects. Then we need write no more than

$$\sin\sigma = R_x\left(1-\frac{\alpha}{R_x^0}\cos\theta\right) \tag{19}$$

We will see later that, despite the low values of α considered here, the effect of the incidence is far from negligible.

The definition of M_∞, $M_\infty^2=(\rho_\infty V_\infty^2/\gamma p_\infty)$ shows that, under hypothesis (2), the conditions across the shock depend on p_∞ only by way of a linear disturbance in $(1/M_\infty^2 R_x^2)$ (Ref. 6).

The base flow is assumed to be given correctly by the self-similar solutions provided by the equivalence principle, for which the equation of the shock is given by

$$R_0=\frac{\tau L}{2\xi_0'}\left(\frac{x}{L}\right)^n \tag{20}$$

in which ξ_0' is a positive constant, less than unity. Dimensional analysis and order of magnitude considerations[11] show that R can be written as

$$R=R_0\left[1+\frac{\alpha}{R_{0x}}\,\xi_1(\theta,n,\gamma)+\frac{1}{M_\infty^2R_x^2}\,\xi_2(n,\gamma)\right]$$

The same result holds for all unknowns of the problem apart from the fact that they also depend on r, which introduces a dimensionless variable ξ proportional to $(r/\tau L)\,(L/x)^n$.

The conditions across the shock can be used to determine explicitly the θ dependency of the function of subscript 1.[11]

Finally, by taking as variables

$$\eta=\frac{\alpha x}{R_0}=n\,\frac{\alpha}{R_{0x}}=\frac{2\xi_0'\alpha}{\tau}\left(\frac{x}{L}\right)^{(1-n)}\quad\text{and}\quad\zeta=\frac{n^2}{M_\infty^2R_x^2} \tag{21}$$

we write the solution in the form

$$R=\frac{\tau L}{2\xi_0'}\left(\frac{x}{L}\right)^n(1+\eta\xi_1\cos\theta+\zeta\xi_2)$$

$$R'=\frac{\tau L}{2}\left(\frac{x}{L}\right)^n$$

$$\xi=\frac{2r\xi_0'}{\tau L}\left(\frac{L}{x}\right)^n$$

$$u=\frac{2nV_\infty}{\gamma+1}\,\frac{r}{x}(u_0+\eta u_1\cos\theta+\zeta u_2) \tag{22}$$

$$v=\frac{2nV_\infty}{\gamma+1}\,\frac{r}{x}(\eta v_1\sin\theta)$$

$$\rho=\frac{\gamma+1}{\gamma-1}\,\rho_\infty(\rho_0+\eta\rho_1\cos\theta+\zeta\rho_2)$$

$$p=\frac{2n^2\rho_\infty V_\infty^2}{\gamma+1}\,\frac{r^2}{x^2}\,(p_0+\eta p_1\cos\theta+\zeta p_2)$$

We see that ξ varies between $1+\eta\xi_1\cos\theta+\zeta\xi_2$ on Σ and ξ_0' on Σ'. The terms of subscript 0, 1, and 2 are functions of ξ, except for ξ_0', ξ_1, and ξ_2, which are constants, and ξ_0, which is introduced for the shock equation to be written $\xi=1$ in the self-similar solution. Small disturbance hypotheses are expressed by

$$\eta\ll 1\quad\text{and}\quad\zeta\ll 1 \tag{23}$$

III. Solution

The solution (23) must verify the general equations for any value of θ, η, and ζ. It is observed that the equations are identically verified for any θ, which validates the form (23) and reduces the problem to three ordinary differential systems. This gives us the problem of the noninstantaneous explosion of an infinite rectilinear wire for the variables of subscript 0, which we can put in the form[11]:

$$\frac{\mathrm{d}z_0}{\mathrm{d}u_0}=G_1(u_0,z_0)$$

$$\frac{\mathrm{d}\log\xi}{\mathrm{d}u_0}=G_2(u_0,z_0) \tag{24}$$

$$\frac{\mathrm{d}\log\rho_0}{\mathrm{d}\log\xi}=G_3(u_0,z_0)$$

where

$$z_0=\gamma\,\frac{p_0}{\rho_0} \tag{25}$$

and the G functions are given by

$$G_1=\frac{2z_0\left[\left(u_0-\frac{\gamma+1}{2}\right)^2\left(\gamma u_0-\frac{\gamma+1}{2n}\right)-\frac{\gamma-1}{2}\,u_0\left(u_0-\frac{\gamma+1}{2n}\right)\left(u_0-\frac{\gamma+1}{2}\right)\right]}{\left(u_0-\frac{\gamma+1}{2}\right)\left\{u_0\left(u_0-\frac{\gamma+1}{2n}\right)\left(u_0-\frac{\gamma+1}{2}\right)+\frac{\gamma-1}{2}\,z_0\left[\frac{(1-n)(\gamma+1)}{\gamma n}-2u_0\right]\right\}}$$

$$-\frac{(\gamma-1)z_0\left\{u_0+\frac{(\gamma+1)[n(1-\gamma)-1]}{2\gamma n}\right\}}{\left(u_0-\frac{\gamma+1}{2}\right)\left\{u_0\left(u_0-\frac{\gamma+1}{2n}\right)\left(u_0-\frac{\gamma+1}{2}\right)+\frac{\gamma-1}{2}\,z_0\left[\frac{(1-n)(\gamma+1)}{\gamma n}-2u_0\right]\right\}}$$

$$G_2=\frac{(\gamma-1)z_0-2\left(u_0-\frac{(\gamma+1)}{2}\right)^2}{2\left\{u_0\left(u_0-\frac{\gamma+1}{2n}\right)\left(u_0-\frac{\gamma+1}{2}\right)+\frac{\gamma-1}{2}\,z_0\left[\frac{(1-n)(\gamma+1)}{\gamma n}-2u_0\right]\right\}}$$

$$G_3=\left(-2u_0-\frac{1}{G_2}\right)\left(u_0-\frac{\gamma+1}{2}\right)^{-1}$$

For the functions of subscript 1, we find that the problem is verified for any θ if

$$
\begin{aligned}
&\left\{\xi^2\left[\rho_0 u_1+\rho_1\left(u_0-\frac{\gamma+1}{2}\right)\right]\right\}_\xi+\xi\rho_0 v_1 \\
&\quad+\frac{(n+1)(\gamma+1)}{2n}\,\xi\rho_1=0 \\
&\left\{\xi^3\left[\rho_0 u_0 u_1+(\rho_0 u_1+\rho_1 u_0)\left(u_0-\frac{\gamma+1}{2}\right)+\frac{\gamma-1}{2}\,p_1\right]\right\}_\xi \\
&\quad+\xi^2\rho_0 u_0 v_1+\xi^2(\gamma+1)(\rho_0 u_1+\rho_1 u_0)-\frac{(\gamma-1)}{2}\,\xi^2 p_1=0 \\
&\left[\xi^3\rho_0 v_1\left(u_0-\frac{\gamma+1}{2}\right)\right]_\xi(\gamma+1)\xi^2\rho_0 v_1+\xi^2\rho_0 u_0 v_0 \\
&\quad-\frac{\gamma-1}{2}\,\xi^2 p_1=0 \\
&\left\{\xi^2\left[\rho_0 s_0 u_1+(\rho_0 s_1+\rho_1 s_0)\left(u_0-\frac{\gamma+1}{2}\right)\right]\right\}_\xi \\
&\quad+\frac{(n+1)(\gamma+1)}{2n}\,\xi(\rho_0 s_1+\rho_1 s_0)+\xi\rho_0 s_0 v_1 \\
&\quad+2\xi\left[\rho_0 u_1+\rho_1\left(u_0-\frac{(\gamma+1)}{2n}\right)\right]=0
\end{aligned}
\tag{26}
$$

where we have let

$$
s_0=\log\frac{p_0}{\rho_0^\gamma}, \qquad s_1=\frac{p_1}{p_0}-\frac{\rho_1}{\gamma\rho_0} \tag{27}
$$

For the terms of subscript 2, we have

$$
\begin{aligned}
&\left\{\xi^2\left[\rho_0 u_2+\rho_2\left(u_0-\frac{\gamma+1}{2}\right)\right]\right\}_\xi+\frac{\gamma+1}{n}\,\xi\rho_2=0 \\
&\left\{\xi^3\left[\rho_0 u_0 u_2+(\rho_0 u_2+\rho_2 u_0)\left(u_0-\frac{\gamma+1}{2}\right)+\frac{\gamma-1}{2}\,p_2\right]\right\}_\xi \\
&\quad+\frac{(n+1)(\gamma+1)}{2n}\xi^2(\rho_0 u_2+\rho_2 u_0)-\frac{(\gamma-1)}{2}\,\xi^2 p_2=0 \\
&\left\{\xi^2\left[\rho_0 s_0 u_2+(\rho_0 s_2+\rho_2 s_0)\left(u_0-\frac{\gamma+1}{2}\right)\right]\right\}_\xi \\
&\quad+\frac{\gamma+1}{n}\,\xi(\rho_0 s_2+\rho_2 s_0)+2\xi\left[\rho_0 u_2+\rho_2\left(u_0-\frac{(\gamma+1)}{2n}\right)\right]=0
\end{aligned}
\tag{28}
$$

where we have let

$$
s_2=\frac{p_2}{p_0}-\gamma\,\frac{\rho_2}{\rho_0} \tag{29}
$$

The difficulty in solving this resides in the fact that the initial integration conditions of the systems (25), (27), and (29) are given on the shock, the position of which is one of the unknowns of the problem. To get around this difficulty, let us make the variable change:

$$
\xi=\bar\xi+\eta\xi_1\,\frac{\bar\xi-\xi_0'}{1-\xi_0'}+\zeta\xi_2\,\frac{\bar\xi-\xi_0'}{1-\xi_0'} \tag{30}
$$

In fact, $\bar\xi$ is the zeroth-order approximation of ξ, equal to one on the shock and to ξ_0' on the body. The previous systems of equations, written in $\bar\xi$, remain formally identical because the order-one terms in η and ζ introduced by the expansions of the system (25) are identically zero since they are proportional to the derivatives in ξ of the equations of system (25). The advantage of this change of variable is therefore that it reduces the conditions on the shock to $\bar\xi=1$ without changing the systems to be solved. We will thus have, in $\bar\xi=1$,

$$
\rho_0=u_0=p_0=1 \quad \text{and} \quad z_0=\gamma \tag{31}
$$

$$
\begin{aligned}
\rho_1+\xi_1\rho_{0\xi}&=0 \\
u_1+\xi_1 u_{0\xi}&=\frac{1-n}{n}\,\xi_1+\frac{\gamma-1}{2n} \\
v_1&=\xi_1-\frac{\gamma+1}{2n} \\
p_1+\xi_1 p_{0\xi}&=\frac{2(1-n)}{n}\,\xi_1-\frac{2}{n}
\end{aligned}
\tag{32}
$$

and

$$
\begin{aligned}
\rho_2+\xi_2\rho_{0\xi}&=-\frac{2}{(\gamma-1)n^2} \\
u_2+\xi_2 u_{0\xi}&=\frac{2(1-n)}{n}\,\xi_2-\frac{1}{n^2} \\
p_2+\xi_2 p_{0\xi}&=\frac{4(1-n)}{n}\,\xi_2-\frac{\gamma-1}{2\gamma n^2}
\end{aligned}
\tag{33}
$$

On the order of approximation chosen here, the functions $\rho_i(\xi)$, $p_i(\xi)$, $u_i(\xi)$, and $v_i(\xi)$ for $i=1{,}2$ can be identified with the calculated functions $\rho_i(\bar\xi)$, $p_i(\bar\xi)$, $u_i(\bar\xi)$, and $v_1(\bar\xi)$. On the other hand, for the base flow, taking ρ_0 as an example, we have $\rho_0(\xi)$, $\rho_0(\bar\xi)+\Delta(\eta\xi_1\cos\theta+\zeta\xi_2)\rho_{0\bar\xi}$, in which $\Delta=(\xi-\xi_0')/(1-\xi_0')$. Finally, we will give the results in the form

$$
\begin{aligned}
u&=\left[\frac{n\tau}{(\gamma+1)\xi_0'}\right]\left[\left(\frac{x}{L}\right)^{n-1}V_\infty(u_0^*+\eta u_1^*\cos\theta+\zeta u_2^*)\right] \\
v&=\left[\frac{n\tau}{(\gamma+1)\xi_0'}\right]\left(\frac{x}{L}\right)^{n-1}V_\infty\eta v_1^*\sin\theta \\
\rho&=\frac{\gamma+1}{\gamma-1}\,\rho_\infty(\rho_0^*+\eta\rho_1^*\cos\theta+\zeta\rho_2^*) \\
p&=\left[\frac{n^2\tau^2}{2(\gamma+1)\xi_0'^2}\right]\left(\frac{x}{L}\right)^{2(n-1)}\rho_\infty V_\infty^2(p_0^*+\eta p_1^*\cos\theta+\zeta p_2^*)\Bigg]
\end{aligned}
\tag{34}
$$

in which the starred quantities are the following functions of $\bar\xi$:

$$
\begin{aligned}
\rho_0^*(\bar\xi)&=\rho_0(\bar\xi) \\
p_0^*(\bar\xi)&=\bar\xi^2 p_0(\bar\xi) \\
u_0^*(\bar\xi)&=\bar\xi u_0(\bar\xi)
\end{aligned}
$$

$$
\begin{aligned}
\rho_1^*(\bar\xi)&=\rho_1(\bar\xi)+\Delta\rho_{0\bar\xi}(\bar\xi) \\
p_1^*(\bar\xi)&=\bar\xi^2 p_1(\bar\xi)+\bar\xi\Delta[\bar\xi p_{0\bar\xi}(\bar\xi)+2p_0(\bar\xi)] \\
u_1^*(\bar\xi)&=\bar\xi u_1(\bar\xi)+\Delta[\bar\xi u_{0\bar\xi}(\bar\xi)+u_0(\bar\xi)] \\
v_1^*(\bar\xi)&=\bar\xi v_1(\bar\xi)
\end{aligned}
$$

$$
\begin{aligned}
\rho_2^*(\bar\xi)&=\rho_2(\bar\xi)+\Delta\rho_{0\bar\xi}(\bar\xi) \\
p_2^*(\bar\xi)&=\bar\xi^2 p_2(\bar\xi)+\bar\xi\Delta[\bar\xi p_{0\bar\xi}(\bar\xi)+2p_0(\bar\xi)] \\
u_2^*(\bar\xi)&=\bar\xi u_2(\bar\xi)+\Delta[\bar\xi u_{0\bar\xi}(\bar\xi)+u_0(\bar\xi)]
\end{aligned}
$$

Equation (31) yields ξ.

The constant ξ_0' is obtained by assigning the nonpenetration condition to the surface for the base solution $u_0(\xi_0') = (\gamma+1)/2$. The equivalence principle is used for calculating ξ_0. By expressing the identity between the released energy per unit length of explosive wire and the obstacle drag for the self-similar solution, we get

$$\xi_0^4 = \frac{(2n-1)(\gamma+1)}{2\pi n^3 \xi_0'^4 p_0'} \tag{35}$$

Analogous formulas were obtained by Merlen and Dyment for the noninstantaneous finite point explosion.[14]

We get the missing equations for ξ_1 and ξ_2 by expressing the resultant of the forces along the x axis on an element $d\Sigma'$ of the surface Σ' bounded by two infinitely close planes $x = \text{const}$ and by a plane angle of $d\theta$ (Fig. 2). This is calculated first by integrating the pressures over $d\Sigma'$ and then applying the momentum theorem to the volume element contiguous to $d\Sigma'$, bounded by the same plane angle and the same planes as $d\Sigma'$ and by the shock (Fig. 2):

$$i\int_{\Sigma_T} (\rho V) V n \, dS = -i\int_{\Sigma_T} p n \, dS \tag{36}$$

Considering the approximations, as well as Eqs. (23), (16), and the mass conservation equation

$$\int_{\Sigma_T} (\rho V) n \, dS = 0$$

we find after a few intricate calculations

$$\int_{\xi_0'}^{1} (p_0 + \rho_0 u_0^2)\xi^3 \, d\xi = \frac{n(\gamma-1)}{2(2n-1)} \xi_0'^4 p_0' \tag{37}$$

which is equivalent to Eq. (36)

$$\int_{\xi_0'}^{1} \Bigg[(3n-1)(p_1 + \rho_1 u_0^2 + 2\rho_0 u_0 u_1) + \frac{2n}{\gamma+1}(\gamma p_0 + \rho_0 u_0^2) v_1 \Bigg] \xi^3 \, d\xi + 2(3n-1)\xi_1 - n(\gamma-1)\xi_0'^4 p_1' = E_1(\xi_1) = 0 \tag{38}$$

$$\int_{\xi_0'}^{1} (p_2 + \rho_2 u_0^2 + 2\rho_0 u_0 u_2)\xi^3 \, d\xi - \frac{\gamma+1}{4\gamma n^2} + 2\xi_2 - \frac{\gamma-1}{2} p_2' \xi_0'^4 = E_2(\xi_2) = 0 \tag{39}$$

The problem comes down to obtaining the zeros of the functions E_1 and E_2, which is solved by a Newton method. The conditions on the shock provide a coupling between these functions and the differential systems, which are integrated by a Runge-Kutta method.

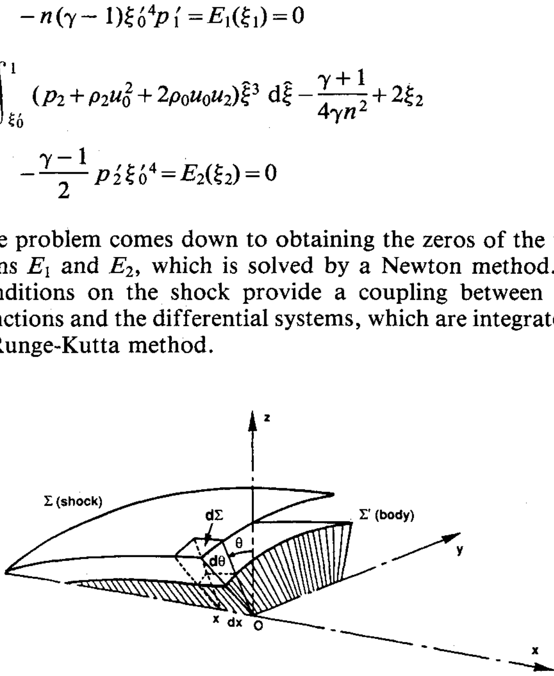

Fig. 2 Integration domain for Eq. (36).

IV. Aerodynamic Coefficients

Starting with the definition

$$C_p = \frac{p' - p_\infty}{\tfrac{1}{2}\rho_\infty V_\infty^2} \tag{40}$$

we get

$$C_p = \frac{(2n-1)\tau^2}{2\pi n \xi_0^4 \xi_0'^4} \left[\left(\frac{x}{L}\right)^{2(n-1)} + 2\frac{\alpha}{\tau}\frac{p_1'\xi_0'}{p_0'}\left(\frac{x}{L}\right)^{(n-1)} \cos\theta \right] + \zeta \frac{n^2\tau^2}{\gamma+1}\left(\frac{x}{L}\right)^{2(n-1)} p_2' - \frac{2}{\gamma M_\infty^2} \tag{41}$$

The calculation shows that to get a correct value for C_p it is not quite right to identify ζ with its first appproximation $\zeta_0 = (4\xi_0'^2/M_\infty^2\tau^2)(x/L)^{2(n-1)}$. In fact, as the values for ξ_1 are very small compared with unity, the expression for ζ can be assimilated to $\zeta = (n^2/R_{0x}^2 M_\infty^2\{1 + [2(2-n)\xi_2/n]\zeta\})$. Solving this equation, we get

$$\zeta = \frac{\zeta_0}{1 + \tfrac{1}{2}(\sqrt{1 + [8\zeta_0(2-n)\xi_2/n]} - 1)} \tag{42}$$

Considering this formula and writing Eq. (42) in the form

$$\frac{C_p}{\tau^2} = C_{p0}\left(\frac{x}{L}\right)^{2(n-1)} + C_{p1}\frac{\alpha}{\tau}\left(\frac{x}{L}\right)^{(n-1)} \cos\theta + \zeta\frac{n^2}{\gamma+1}\left(\frac{x}{L}\right)^{2(n-1)} p_2' - \frac{2}{\gamma M_\infty^2 \tau^2}$$

we get the values of C_{p0} and C_{p1} in Tables 1–3, for $\gamma = 1.4$ and $n = 1$, ¾, and ⅔.

The nose drag, without considering the base, is defined by

$$F_x = \int_0^{2\pi}\int_0^L (p' - p_\infty) R_x' R' \, dx \, d\theta \tag{43}$$

We take as reference area the maximum cross section of the nose, which is

$$S_{\text{ref}} = \pi R'^2(L) = \frac{\pi L^2}{4}\tau^2 \tag{44}$$

and we define the drag coefficient by

$$C_x = \frac{F_x}{\tfrac{1}{2}\rho_\infty V_\infty S_{\text{ref}}} \tag{45}$$

If we write

$$\frac{C_x}{\tau^2} = C_{x0} + \frac{C_{x2}}{M_\infty^2 \tau^2} \tag{46}$$

C_{x0} is a constant given by $C_{x0} = (1/2\pi\xi_0'^4\xi_0^4)$ and the effect of p_∞ is given by

$$C_{x2} = \frac{2n^3}{\gamma+1} M_\infty^2 \tau^2 p_2' \int_0^L \left(\frac{\hat{x}}{L}\right)^{4n-3} \zeta \, d\left(\frac{\hat{x}}{L}\right) - \frac{2}{\gamma} \tag{47}$$

The numerical data for the same three noses and $\gamma = 1.4$ can be found in Tables 1–3.

Each slice of the obstacle defined by $x = \text{const}$ contributes to the drag, the distribution of which per unit length along the x axis can be given in a first approximation by

$$f_x = \tfrac{1}{2}\rho_\infty V_\infty^2 \left[\frac{\tau^4}{4\xi_0^4 \xi_0'^4} (2n-1) L \left(\frac{x}{L}\right)^{4n-3} \right]$$

Table 1 Numerical values for $n = 0.6667$ and $\gamma = 1.4$

ξ	ρ_0^*	u_0^*	p_0^*	Ψ_0	Φ_1	ρ_1^*	u_1^*	v_1^*	p_1^*	Ψ_1	ρ_2^*	u_2^*	p_2^*	Ψ_2
1.0000	1.0000	1.0000	1.0000	−0.2000	0.0000	0.0000	0.5175	−1.6550	−2.5650	0.1820	−11.2500	−0.3854	3.4078	−0.3729
0.9764	0.8528	0.9936	0.9292	−0.1483	0.1940	−0.4860	0.4333	−1.5380	−2.6704	0.1928	−7.0816	−0.3820	3.6259	−0.5322
0.9579	0.7485	0.9906	0.8831	−0.1140	0.3460	−0.7416	0.3727	−1.4555	−2.7127	0.1833	−4.6025	−0.3698	3.6681	−0.5548
0.9431	0.6699	0.9894	0.8511	−0.0899	0.4699	−0.8841	0.3271	−1.3959	−2.7277	0.1678	−3.0091	−0.3528	3.6460	−0.5273
0.9309	0.6080	0.9891	0.8279	−0.0724	0.5739	−0.9653	0.2913	−1.3529	−2.7301	0.1512	−1.9294	−0.3336	3.6002	−0.4827
0.9208	0.5577	0.9894	0.8106	−0.0593	0.6632	−1.0107	0.2626	−1.3227	−2.7266	0.1356	−1.1691	−0.3136	3.5474	−0.4344
0.9123	0.5158	0.9900	0.7972	−0.0493	0.7413	−1.0344	0.2391	−1.3024	−2.7205	0.1214	−0.6198	−0.2939	3.4949	−0.3880
0.9050	0.4802	0.9907	0.7867	−0.0414	0.8109	−1.0444	0.2195	−1.2901	−2.7132	0.1089	−0.2132	−0.2749	3.4456	−0.3455
0.8988	0.4495	0.9915	0.7782	−0.0352	0.8736	−1.0455	0.2028	−1.2845	−2.7058	0.0979	0.0926	−0.2510	3.4006	−0.3077
0.8911	0.4106	0.9927	0.7685	−0.0280	0.9580	−1.0371	0.1821	−1.2859	−2.6950	0.0840	0.4204	−0.2324	3.3411	−0.2591
0.8867	0.3884	0.9935	0.7634	−0.0243	1.0091	−1.0274	0.1705	−1.2922	−2.6884	0.0761	0.5774	−0.2175	3.3077	−0.2317
0.8811	0.3594	0.9946	0.7573	−0.0199	1.0800	−1.0094	0.1557	−1.3082	−2.6795	0.0660	0.7490	−0.1972	3.2638	−0.1969
0.8751	0.3270	0.9960	0.7513	−0.0155	1.1662	−0.9822	0.1395	−1.3344	−2.6693	0.0553	0.8962	−0.1738	3.2163	−0.1600
0.8703	0.3001	0.9971	0.7469	−0.0123	1.2456	−0.9539	0.1264	−1.3794	−2.6608	0.0468	0.9832	−0.1539	3.1789	−0.1315
0.8647	0.2673	0.9986	0.7422	−0.0090	1.3562	−0.9125	0.1109	−1.4515	−2.6509	0.0372	1.0464	−0.1296	3.1366	−0.0999
0.8599	0.2370	0.9999	0.7386	−0.0065	1.4771	−0.8676	0.0970	−1.5492	−2.6422	0.0292	1.0633	−0.1076	3.1018	−0.0744
0.8550	0.2041	1.0013	0.7355	−0.0043	1.6413	−0.8113	0.0823	−1.7058	−2.6337	0.0215	1.0317	−0.0845	3.0693	−0.0510
0.8502	0.1670	1.0028	0.7328	−0.0025	1.8952	−0.7383	0.0664	−1.9824	−2.6253	0.0142	0.9556	−0.0604	3.0399	−0.0303
0.8456	0.1244	1.0043	0.7308	−0.0011	2.3655	−0.6415	0.0488	−2.5453	−2.6178	0.0077	0.7959	−0.0363	3.0161	−0.0138
0.8410	0.0672	1.0058	0.7294	−0.0002	3.9687	−0.4838	0.0259	−4.5526	−2.6113	0.0021	−0.4804	−0.0120	2.9995	−0.0026
0.8388	0.0036	1.0065	0.7291	0.0000	68.4753	0.0000	−0.0014	−83.6417	−2.6089	0.0000	0.0000	0.0002	2.9957	0.0000

ξ_0	0.9567	C_{x0}	0.3822
ξ_0'	0.8388	C_{x2}	0.107
ξ_1	0.1450	C_z/α	1.725
ξ_2	0.9323	C_m/α	0.739
C_{p0}	0.1918	$z_A/L\alpha$	−0.600
C_{p1}	−1.1514		

Table 2 Numerical values for $n = 0.75$ and $\gamma = 1.4$

ξ	ρ_0^*	u_0^*	p_0^*	Ψ_0	Φ_1	ρ_1^*	u_1^*	v_1^*	p_1^*	Ψ_1	ρ_2^*	u_2^*	p_2^*	Ψ_2
1.0000	1.0000	1.0000	1.0000	−0.2000	0.0000	0.0000	0.2893	−1.5830	−2.6214	0.2218	−8.8889	−0.4323	2.4370	−0.3229
0.9848	0.9366	1.0030	0.9732	−0.1648	0.1233	−0.1936	0.2476	−1.5026	−2.6645	0.2039	−7.4496	−0.4031	2.5145	−0.3652
0.9717	0.8821	1.0063	0.9518	−0.1369	0.2338	−0.3375	0.2138	−1.4332	−2.6906	0.1850	−6.2905	−0.3737	2.5604	−0.3765
0.9604	0.8343	1.0096	0.9345	−0.1145	0.3335	−0.4466	0.1861	−1.3731	−2.7059	0.1664	−5.3405	−0.3450	2.5853	−0.3698
0.9507	0.7919	1.0128	0.9202	−0.0963	0.4242	−0.5304	0.1630	−1.3211	−2.7143	0.1490	−4.5510	−0.3117	2.5963	−0.3529
0.9422	0.7540	1.0159	0.9084	−0.0815	0.5069	−0.5955	0.1436	−1.2761	−2.7183	0.1331	−3.8876	−0.2916	2.5979	−0.3308
0.9348	0.7197	1.0189	0.8985	−0.0693	0.5829	−0.6463	0.1272	−1.2373	−2.7193	0.1187	−3.3251	−0.2673	2.5933	−0.3062
0.9284	0.6885	1.0216	0.8902	−0.0591	0.6530	−0.6861	0.1133	−1.2041	−2.7186	0.1058	−2.8445	−0.2447	2.5848	−0.2812
0.9228	0.6600	1.0241	0.8832	−0.0507	0.7179	−0.7173	0.1013	−1.1759	−2.7167	0.0944	−2.4311	−0.2239	2.5740	−0.2567
0.9178	0.6338	1.0264	0.8773	−0.0436	0.7782	−0.7417	0.0909	−1.1521	−2.7141	0.0842	−2.0737	−0.2048	2.5619	−0.2374
0.9135	0.6097	1.0285	0.8722	−0.0377	0.8344	−0.7606	0.0820	−1.1323	−2.7112	0.0753	−1.1631	−0.1874	2.5492	−0.2117
0.9097	0.5873	1.0304	0.8678	−0.0327	0.8872	−0.7752	0.0741	−1.1161	−2.7082	0.0674	−1.4921	−0.1714	2.5366	−1.1917
0.9048	0.5566	1.0329	0.8625	−0.0266	0.9605	−0.7905	0.0642	−1.0977	−2.7037	0.0572	−1.1471	−0.1501	2.5183	−0.1649
0.9007	0.5289	1.0351	0.8582	−0.0218	1.0279	−0.7998	0.0560	−1.0857	−2.6994	0.0488	−0.8624	−0.1317	2.5014	−0.1418
0.8963	0.4960	1.0375	0.8537	−0.0169	1.1102	−0.8054	0.0471	−1.0779	−2.6943	0.0397	−0.5563	−0.1109	2.4814	−0.1160
0.8913	0.4534	1.0403	0.8490	−0.0118	1.2213	−0.8041	0.0370	−1.0807	−2.6881	0.0295	−0.2144	−0.0864	2.4570	−0.0865
0.8871	0.4120	1.0427	0.8454	−0.0080	1.3372	−0.7937	0.0287	−1.1007	−2.6826	0.0214	0.0607	−0.0656	2.4359	−0.0622
0.8830	0.3600	1.0452	0.8421	−0.0046	1.5004	−0.7681	0.0202	−1.1574	−2.6768	0.0134	0.3255	−0.0438	2.4141	−0.0382
0.8191	0.2897	1.0476	0.8395	−0.0019	1.7798	−0.7112	0.0115	−1.3165	−2.6714	0.0062	0.5439	−0.0224	2.3938	−0.0168
0.8751	0.0076	1.0501	0.8377	0.0000	53.2545	0.0000	0.0000	−45.2322	−2.6665	0.0000	0.0000	−0.0000	2.3773	0.0000

ξ_0	0.9166	C_{x0}	0.385
ξ_0'	0.8751	C_{x2}	0.202
ξ_1	0.0170	C_z/α	1.907
ξ_2	0.8073	C_m/α	0.763
C_{p0}	0.2564	$z_A/L\alpha$	−0.693
C_{p1}	−1.4285		

The point of application b of the drag on each slice is defined by

$$\frac{z_b f_x}{\frac{1}{2}\rho_\infty V_\infty^2} = \int_0^{2\pi} C_p R_x' R'^2 \cos\theta \, d\theta$$

In the integral on the right, only the subscript 1 terms do not cancel out, so we get

$$z_b = \alpha x \frac{p_1' \xi_0'}{2 p_0'} \tag{48}$$

Calculating this shows that p_1 is negative, so the drag is applied below the x axis if α is positive. The ordinate of the point A at which the aerodynamic forces are applied is given by

$$F_x z_A = \int_0^L z_b f_x \, dx$$

whence

$$z_A = \frac{(2n-1)L}{4n-1} \frac{p_1' \xi_0'}{p_0'} \alpha \tag{49}$$

So there exists a drag-induced pitching moment. By taking $S_{\rm ref}$ and L as the reference area and length, and with the axis conventions of Fig. 1, we can calculate the coefficient C_{mx} of

Table 3 Numerical values for $n = 1.00$ and $\gamma = 1.4$

ξ	$\rho_0'^*$	$u_0'^*$	$p_0'^*$	Ψ_0	Φ_1	$\rho_1'^*$	$u_1'^*$	$v_1'^*$	$p_1'^*$	Ψ_1	$\rho_2'^*$	$u_2'^*$	$p_2'^*$	Ψ_2
1.0000	1.0000	1.0000	1.0000	−0.2000	0.0000	0.0000	0.1467	−1.2533	−2.1066	0.0213	−5.0000	−0.5431	0.7710	−0.0914
0.9962	1.0031	1.0044	1.0043	−0.1910	0.0240	−0.0056	0.1394	−1.2376	−2.1183	0.0196	−4.9554	−0.5138	0.7953	−0.0837
0.9925	1.0059	1.0087	1.0083	−0.1820	0.0487	−0.0107	0.1322	−1.2214	−2.1293	0.0180	−4.9140	−0.4852	0.8183	−0.0764
0.9888	1.0087	1.0130	1.0122	−0.1731	0.0743	−0.0156	0.1251	−1.2047	−2.1397	0.0164	−4.8756	−0.4572	0.8401	−0.0695
0.9851	1.0113	1.0172	1.0158	−0.1643	0.1008	−0.0200	0.1182	−1.1874	−2.1494	0.0149	−4.8399	−0.4298	0.8607	−0.0628
0.9814	1.0137	1.0214	1.0192	−0.1554	0.1285	−0.0241	0.1113	−1.1694	−2.1586	0.0134	−4.8067	−0.4027	0.8801	−0.0565
0.9777	1.0160	1.0256	1.0224	−0.1467	0.1570	−0.0279	0.1046	−1.1509	−2.1672	0.0121	−4.7761	−0.3762	0.8983	−0.0506
0.9741	1.0181	1.0297	1.0254	−0.1380	0.1866	−0.0314	0.0980	−1.1316	−2.1752	0.0108	−4.7479	−0.3501	0.9154	−0.0450
0.9705	1.0201	1.0338	1.0283	−0.1294	0.2175	−0.0347	0.0916	−1.1117	−2.1826	0.0096	−4.7219	−0.3244	0.9313	−0.0398
0.9669	1.0220	1.0379	1.0309	−0.1209	0.2499	−0.0376	0.0852	−1.0909	−2.1895	0.0084	−4.6979	−0.2988	0.9463	−0.0349
0.9633	1.0237	1.0419	1.0333	−0.1125	0.2836	−0.0403	0.0789	−1.0693	−2.1959	0.0073	−4.6760	−0.2736	0.9600	−0.0303
0.9598	1.0253	1.0459	1.0356	−0.1041	0.3190	−0.0427	0.0728	−1.0469	−2.2017	0.0064	−4.6561	−0.2487	0.9727	−0.0261
0.9563	1.0268	1.0499	1.0377	−0.0958	0.3562	−0.0449	0.0667	−1.0234	−2.2070	0.0054	−4.6380	−0.2241	0.9843	−0.0223
0.9528	1.0281	1.0539	1.0396	−0.0877	0.3956	−0.0469	0.0608	−0.9989	−2.2118	0.0046	−4.6217	−0.1996	0.9949	−0.0187
0.9493	1.0293	1.0578	1.0413	−0.0795	0.4377	−0.0486	0.0550	−0.9729	−2.2162	0.0038	−4.6069	−0.1751	1.0046	−0.0155
0.9459	1.0304	1.0617	1.0429	−0.0715	0.4824	−0.0501	0.0493	−0.9457	−2.2201	0.0031	−4.5940	−0.1509	1.0131	−0.0126
0.9425	1.0314	1.0656	1.0442	−0.0636	0.5306	−0.0514	0.0437	−0.9168	−2.2235	0.0025	−4.5826	−0.1268	1.0206	−0.0100
0.9392	1.0323	1.0695	1.0455	−0.0558	0.5830	−0.0524	0.0382	−0.8860	−2.2265	0.0019	−4.5727	−0.1028	1.0271	−0.0077
0.9358	1.0330	1.0733	1.0465	−0.0480	0.6410	−0.0533	0.0329	−0.8527	−2.2291	0.0014	−4.5643	−0.0787	1.0326	−0.0058
0.9325	1.0337	1.0772	1.0474	−0.0404	0.7055	−0.0539	0.0277	−0.8168	−2.2313	0.0010	−4.5573	−0.0548	1.0371	−0.0041
0.9293	1.0342	1.0810	1.0482	−0.0328	0.7792	−0.0543	0.0226	−0.7772	−2.2331	0.0007	−4.5518	−0.0309	1.0406	−0.0027
0.9260	1.0346	1.0848	1.0488	−0.0254	0.8664	−0.0545	0.0177	−0.7327	−2.2344	0.0004	−4.5477	−0.0071	1.0431	−0.0016
0.9228	1.0349	1.0885	1.0492	−0.0180	0.9153	−0.0545	0.0129	−0.6810	−2.2355	0.0002	−4.5448	0.0168	1.0447	−0.0008
0.9196	1.0351	1.0923	1.0495	−0.0101	1.1274	−0.0543	0.0084	−0.6167	−2.2361	0.0001	−4.5433	0.0409	1.0452	−0.0003
0.9165	1.0352	1.0960	1.0497	−0.0036	1.4103	−0.0538	0.0041	−0.5231	−2.2365	0.0000	−4.5431	0.0649	1.0447	0.0000
0.9149	1.0352	1.0979	1.0497	−0.0000		−0.0534	0.0021	−0.3992	−2.2365	0.0000	−4.5435	0.0769	1.0441	0.0000

ξ_0	0.8120	C_{x0}	0.5225
ξ_0'	0.9149	C_{x2}	−0.038
ξ_1	−0.0533	C_z/α	2.038
ξ_2	0.4569	C_m/α	0.679
C_{p0}	0.5225	$z_A/L\alpha$	−0.650
C_{p1}	−2.0372		

this moment about the y axis or any axis parallel to it and intersecting the x axis. We get

$$C_{mx} = \frac{\tau^2}{2\pi\xi_0'^4\xi_0^4}\,\frac{(2n-1)}{4n-1}\,\frac{p_1'\xi_0'}{p_0'}\,\alpha \tag{50}$$

We can see that C_{mx} is of the order of $\alpha\tau^2$.

The lift is obtained by the equation

$$F_z = -\int_0^{2\pi}\int_0^L p'R'\cos\theta\,\mathrm{d}x\,\mathrm{d}\theta \tag{51}$$

where only the subscript 1 term is nonzero. With the same reference quantities as for the drag, we get

$$C_z = -\frac{2np_1'\xi_0'}{\gamma+1}\,\alpha \tag{52}$$

which is positive if α is, since p_1 is negative.

By calculating the pitching moment due to the lift, we get the abscissa at which the moment is applied:

$$x_A = \frac{2nL}{2n+1} \tag{53}$$

The pitching coefficient with respect to the point O_L (Fig. 2) is easily found from Eqs. (53) and (54):

$$C_m = -\frac{2np_1'\xi_0'}{(2n+1)(\gamma+1)}\,\alpha \tag{54}$$

This coefficient is positive with α, which confirms the convention of a positive pitching-up moment in the (O_L,x_1,y_1,z_1) reference frame. We see that C_{mx} is negligible compared with C_m. For the three previous nose cones, and for $\gamma = 1.4$, the numerical values of C_x and C_m are given in Tables 1–3.

V. Stream Functions

The effect of the nose blunting on the mass density at the surface is included by using the entropy correction of Hayes and Probstein in an axisymmetrical or two-dimensional configuration. let us recall the principle by letting x_i be the abscissa of the point P where a given streamline cuts through the shock. In the framework of the equivalence principle,[9] we can write the value of (p/ρ^γ) on the shock at x_i (Fig. 3) in the form

$$\frac{p}{\rho^\gamma} = \frac{2(\gamma-1)^\gamma V_\infty^2}{n(\gamma+1)^{\gamma+1}\rho_\infty^{\gamma-1}}\,R_x^2(x_i) = \frac{2(\gamma-1)^\gamma V_\infty^2}{n(\gamma+1)^{\gamma+1}\rho_\infty^{\gamma-1}}\tan^2\sigma_i \tag{55}$$

whereas the straight shock equations must yield

$$\frac{p}{\rho^\gamma} = \frac{2(\gamma-1)^\gamma V_\infty^2}{n(\gamma+1)^{\gamma+1}\rho_\infty^{\gamma-1}}\sin^2\sigma_i \tag{56}$$

If the error induced by substituting Eq. (56) for Eq. (57) in area II is no greater than the approximation error, the entropy of the streamlines in area III is much greater in the modeling than it is in reality. The experiment[9] as well as certain theoretical considerations[5,11] show, as we have seen, that the pressure in area III can be considered, for slightly blunted bodies, equal to the pressure on the body and, for this reason, only ρ has to be corrected. Comparing Eqs. (56) and (57) suggests the following correction[9,11]:

$$\tilde{\rho} = \rho\left(\frac{\cos\sigma}{\cos\sigma_i}\right)^{2/\gamma} \tag{57}$$

For the self-similar solution, using the relation between σ, the first approximation of $R[R_0(x)]$ and the stream function, we get $\tilde{\rho} = K\rho$ with

$$K = \left[\frac{R_{0x}^2([2/(1-\gamma)]\,\rho_0\{u_0 - [(\gamma+1)/2]\}\xi^2)^{n-1/n} + 1}{R_{0x}^2 + 1}\right]^{1/\gamma} \tag{58}$$

We see that K is constant along a given streamline, varying only by negligible terms.

The expression for $\tilde{\rho}$ remains finite and nonzero in $\xi=\xi_0'$. Substituting $\tilde{\rho}$ for ρ, we get a corrected solution that has the same precision for slightly blunted bodies as the self-similar solution, but for which the temperature T remains finite at the surface of the body. In fact, this solution assumes that the shock is a power-law shock and that the stream function remains valid through area I. This fact requires that the body shape be adapted in area I. Nevertheless the principle of the previous correction can be generalized by assigning to the streamlines of area III the entropy that they really have just downstream of area I, which should therefore be calculated independently of the hypotheses of the equivalence principle. However, for slight blunting, these corrections are equivalent. As a matter of fact, the result on the obstacle is always the same since it corresponds to the streamlines passing through the stagnation point where the entropy jump is at its maximum, and it is found by letting $\sigma_i=\pi/2$. For this reason, and considering the thinness of area III, the correction (59) is a very realistic approximation.

Similarly, the subscript 1 and 2 expansions are consistent only if p_1 and p_2 are determined correctly. Yet in Eqs. (27) and (29), ρ_0 appears only in the form of the products $\rho_0 u_1$, $\rho_0 v_1$, and $\rho_0 u_2$. So it must be concluded that these quantities are also determined correctly by our solutions and that the entropy correction also applies to u_1, v_1, and u_2 such that $\rho_0 u_1=\tilde{\rho}_0\tilde{u}_1$, etc. Thus we let $\tilde{u}_1=u_1/K$, $\tilde{v}_1=v_1/K$, and $\tilde{u}_2=u_2/K$. In fact, this is equivalent to assuming that, in the expression for u and v of Eq. (23), we substitute $\tilde{\eta}=\eta/K$ and $\tilde{\zeta}=\zeta/K$ for η and ζ.

To generalize the entropy correction to the three-dimensional case treated here, we have to find two stream functions to determine the coordinates x_i and θ_i of point P.

The method for finding the stream function for the self-similar flow is based on dimensional analysis and can be found in Ref. 15. This can also be applied to find the complete solution, if the body is at zero incidence. The only difference stems from the fact that the dimensional considerations are no longer sufficient, since the flow is no longer self similar. So the form of the stream function as a function of $\tilde{\zeta}$ must be anticipated. It is reasonable to look for it in the form $\psi=\psi_0+\tilde{\zeta}\psi_2$. Considering the fact that K is constant on a given streamline, it is easy to show that

$$\psi=\frac{\gamma+1}{\gamma-1}\rho_\infty r^2\left\{\rho_0\left(u_0-\frac{\gamma+1}{2}\right)+n\tilde{\zeta}\left[\rho_2\left(u_0-\frac{\gamma+1}{2}\right)+\rho_0 u_2\right]\right\}$$

is a stream function.

As soon as the nose is placed at incidence, axisymmetry disappears and the streamlines are no longer two dimensional except for the planes $\theta=0$ and π, where v is zero. For these special cases, the method described for $\alpha=0$ again applies. We are led to

$$\Psi_s=\left(\frac{x}{L}\right)^{2n}\left(\rho_0\left(u_0-\frac{\gamma+1}{2}\right)\xi^2+\frac{2n}{1+n}\tilde{\eta}\cos\theta\left\{\xi^2\left[\rho_1\left(u_0-\frac{\gamma+1}{2}\right)+\rho_0u_1\right]\right\}+n\tilde{\zeta}\left\{\xi^2\left[\rho_2\left(u_0-\frac{\gamma+1}{2}\right)+\rho_0u_2\right]\right\}\right) \tag{59}$$

in which Ψ_s is a dimensionless form of the stream function in the plane of symmetry.

For the other values of θ, the equation of the streamlines is obtained by integrating

$$\frac{\mathrm{d}x}{V_\infty}=\frac{\mathrm{d}r}{u}=\frac{r\,\mathrm{d}\theta}{v}$$

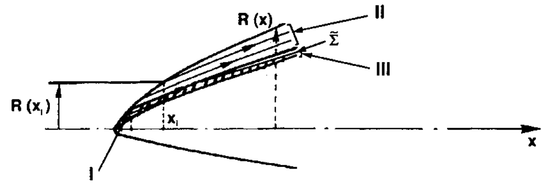

Fig. 3 Structure of the flow. Area I is the flow around the blunted nose. Area II is composed by the streamlines that have crossed the shock with a small deviation. Area III is the wake of area I.

which, in dimensionless form, becomes

$$\frac{\mathrm{d}\xi}{\xi}=\frac{2n}{\gamma+1}\left(u_0-\frac{\gamma+1}{2}+\tilde{\eta}u_1\cos\theta+\tilde{\zeta}u_2\right)\frac{\mathrm{d}x}{x}$$

$$\mathrm{d}\theta=\frac{2n}{\gamma+1}\tilde{\eta}v_1\sin\theta\frac{\mathrm{d}x}{x}$$

Any quantity f that is conserved along a given streamline must therefore verify

$$\frac{\partial f}{\partial x}+\frac{2n}{\gamma+1}\left(u_0-\frac{\gamma+1}{2}+\tilde{\eta}u_1\cos\theta+\tilde{\zeta}u_2\right)\frac{\xi}{x}\frac{\partial f}{\partial\xi}+\frac{2n}{\gamma+1}\frac{\tilde{\eta}}{x}v_1\sin\theta\frac{\partial f}{\partial\theta}=0 \tag{60}$$

We get the general function Ψ by letting $\Psi=\Psi_s Q(\theta)$ and looking for the function Q for which Ψ verifies Eq. (61). Using the order-one mass conservation equation given in Eq. (27) and the order-zero equation, we can verify that Ψ is a dimensionless Lagrangian variable if $Q=|\sin\theta|^{2n/(1+n)}$. So for $\theta\neq 0$ or π

$$\Psi=\left(\frac{x}{L}\right)^{2n}|\sin\theta|^{2n/(1+n)}\Psi_s \tag{61}$$

This function is constant along a streamline. On the shock (Fig. 3), we get

$$\Psi=\frac{1-\gamma}{2}\left(\frac{x_i}{L}\right)^{2n}(|\sin\theta_i|^{(2n/1+n)}\times\left[1+2\tilde{\eta}_i\left(\xi_1-\frac{1}{1+n}\right)\cos\theta_i+2\tilde{\zeta}_i\xi_2\right] \tag{62}$$

which yields a first equation relating ξ, θ, and x to x_i and θ_i.

At the zero order, the second stream function is obviously $\Phi=\theta$. We look for the form $\Phi=\theta+\tilde{\eta}\Phi_1(\xi)\sin\theta$. Writing Eq. (61) for this function Φ, we get a first-order inhomogeneous differential equation for Φ_1. Choosing $\Phi_1=0$ on the shock, and using Eq. (62), the solution yields

$$\Phi=\theta_i=\theta+\tilde{\eta}\Phi_1\sin\theta \tag{63}$$

with

$$\Phi_1=\frac{2}{1-\gamma}\left[\frac{2}{1-\gamma}\rho_0\left(u_0-\frac{\gamma+1}{2}\right)\xi^2\right]^{(1-n)/2n}\times\int_\xi^1\frac{\rho_0v_1\tilde{\xi}}{\left[\frac{2}{1-\gamma}\rho_0\left(u_0-\frac{\gamma+1}{2}\right)\tilde{\xi}^2\right]^{(1+n)/2n}}\mathrm{d}\tilde{\xi} \tag{64}$$

Equation (65) solves the problem of determining θ_i for given x, θ, and ξ so Eq. (63) can be considered as having a single unknown x_i and can be solved with no great difficulty.

To generalize the entropy correction for application here, we now have only to give an exact explicit value of cos σ at all points on the shock or

$$\cos^2\sigma = \frac{\xi_0' + \alpha n\tau \cos\theta (x/L)^{(n-1)}}{\xi_0' + (n^2\tau^2/4\xi_0'^2)(x/L)^{2(n-1)} + (\alpha n\tau/\xi_0')\xi_1 \cos\theta\, (x/L)^{(n-1)} + \{[2n(2-n)\xi_0'\xi_2]/M_\infty^2\}} \tag{65}$$

To determine cos σ_i, this formula has to be applied to x_i and θ_i. In fact, we only have to calculate $(x/L)^{n-1}$ from Eq. (64) for given x, θ, and ξ, as θ_i is known from Eq. (65). To do so, we have to solve Eq. (64) which, considering the expressions for $\tilde{\eta}$ and $\tilde{\zeta}$ given in Eq. (22) because $K=1$ on the shock, leads to

$$\left(\frac{x_i}{L}\right)^{2(n-1)} + \frac{4(n-1)\xi_0'\alpha}{n\tau}\left(\xi_1 - \frac{1}{1+n}\right)\cos\theta_i \left(\frac{x_i}{L}\right)^{(n-1)}$$

$$-\left[(|\sin\theta_i|)^{2(1-n)/1+n}\left(\frac{2\Psi}{1-\gamma}\right)^{(n-1)/n} + \frac{8(1-n)\xi_0'^2\xi_2}{nM_\infty^2\tau^2}\right] = 0$$

It is seen that $(x/L)^{(n-1)}$ is a solution of a second-order equation whose constant term is negative. So there exists only one positive solution giving us the quantity we are looking for. In the tables, Ψ will be written in the form $\Psi = \Psi_0 + \tilde{\eta}\Psi_1 \cos\theta + \tilde{\zeta}\Psi_2$ in which each term is a function of $\tilde{\xi}$.

VI. Results and Discussion

We should first compare our results with others already published. Kubota[6] gives R in the form $R/R' = A[1 + B(x/L)^{2(1-n)}/M_\infty^2\tau^2]$. The identification with our model yields $A = 1/\xi_0'$ and $B = \xi_2\xi_0'$. For $\gamma = 1.4$, the comparisons are given in Table 4.

It is observed that the value of ξ_2 is greater in our calculation, which brings our results somewhat closer to the experimental data.[6] This is partly explained by precision problems, but mainly by the way the subscript 2 problem is solved. Kubota solved it by Sakuraï's linearization technique, in which the problem closure is given by the condition $\rho' = 0$. Yet this condition is very sensitive to the correct determination of ξ_0' because of the high values of $\rho_{0\xi}$ in the vicinity of ξ_0'. The integral condition (40) necessarily leads to $\rho' = 0$ but is not as sensitive to this singularity in the flow.

If we now compare our results for $n = 1$ with those of Doty and Rasmussen, we can compare ξ_1 directly with the parameter g of these authors. For $\gamma = 1.4$, we find $\xi_1 = -0.0533$ whereas they obtain $\xi_1 = -0.057$ for $M_\infty\tau \to \infty$. The difference is minimal and is explained by the fact that we do not use the assumption of constant mass density in the flow. This is verified at 3.5% by the self-similar solution (Table 2). For the coefficient C_z/α, we get 2.038, as against 2.041 for the constant-density solution and 2.044 for Cheng's Newtonian limit.

In the calculation of C_{x0}, our results are identified with those of Cernyi.[3]. That is, we find a minimum for C_{x0} for $n \approx 0.71$ *if* $\gamma > 0.1$. The value of C_{x0} is very sensitive to variations in γ, as Fig. 4a shows. Figure 4 also shows that the minimum tends to be reabsorbed when the subscript 2 term is taken into account. For a value of $M_\infty\tau = 3.62$ corresponding to Kubota's experiments, this local minimum has disappeared, so it is a phenomenon typical of high hypersonics that should not be very convenient to confirm experimentally and even less so in that it is only a part of the total nose drag.

Table 4 Comparison with Kubota $\gamma = 1{,}4$

	Present calculation		Kubota	
n	ξ_0'	ξ_2	ξ_0'	ξ_2
1	0.9149	0.4569	0.9157	0.3959
¾	0.8751	0.8073	0.8749	0.6767
⅔	0.8388	0.9323	0.8389	0.7928

Figure 5 shows the results for C_z and C_m. There aerodynamic coefficients depend closely on the shape of the body. It is observed that the curves all cross in the vicinity of the value

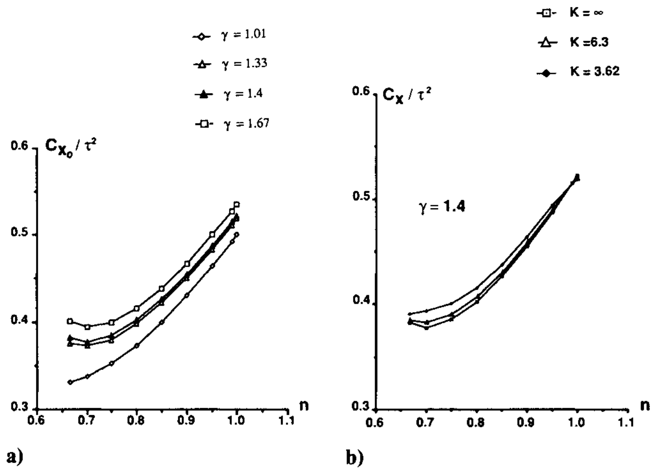

Fig. 4 Drag coefficient vs power-law exponent; a) effect of γ for $M_\infty = \infty$, b) effect of $M_\infty\tau$ on the minimum drag.

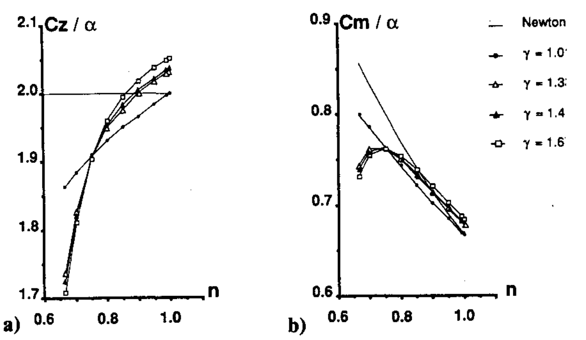

Fig. 5 Lift and pitch coefficients; a) lift coefficient vs power-law exponent, b) pitch coefficient vs power-law exponent.

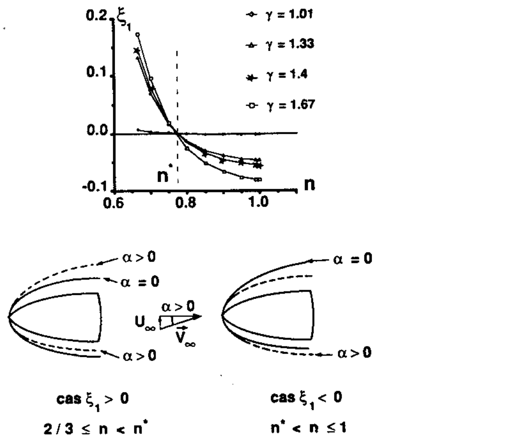

Fig. 6 Incidence effect on the shock position.

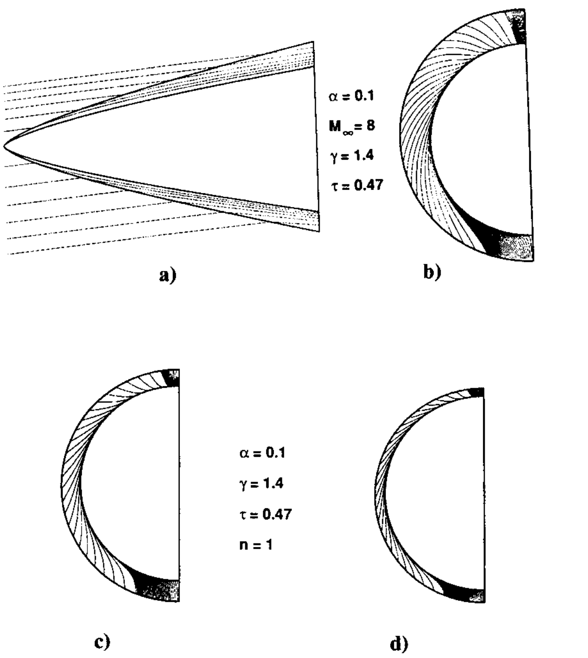

Fig. 7 Stream surfaces; a) streamline in the symmetry plane for $n = 0.7$, b) stream surface Φ in the plane $x = L$ for $n = 0.7$, c) and d) stream surfaces Φ in the plane $x = L$ for $n = 1$ with M_∞ and 25.

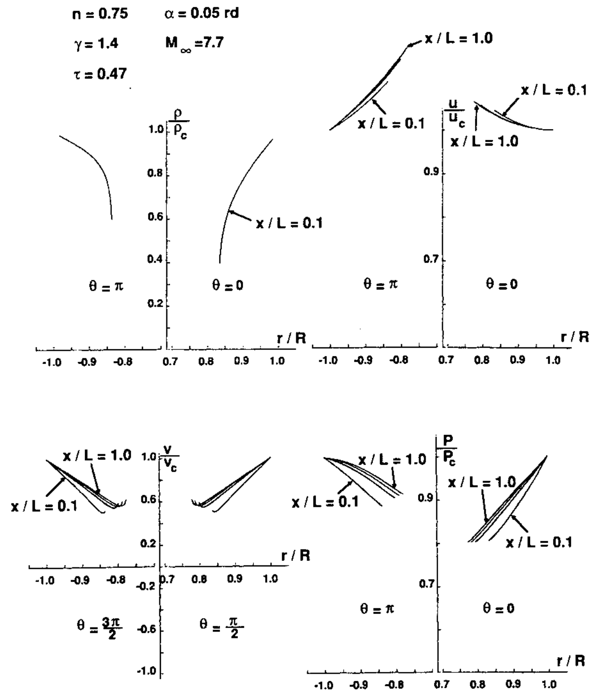

Fig. 8 Repartitions of the flow variables in the shock layer.

$n = n^*$. The tendencies are reversed to either side of this critical value, which corresponds approximately to the C_m maximum and for which the variations in γ do not seem to have any influence on the lifting problem. This observation may be correlated with the variation of the shock position with α, which is illustrated by the $\xi_1(n)$ function presented in Fig. 6. We do in fact see that the shift of the shock position between the cases $\alpha = 0$ and $\alpha > 0$ is of opposite direction according to n is greater or smaller than $n^* \approx 0.75$. Here we come across a phenomenon analogous to what Doty and Rasmussen found for the cone, for which the direction of shift of the shock is reversed for a precise value of $M_\infty \tau$. Here, the direction of this shift depends on the blunted nose size characterized by n.

Doty and Ramussen's results can most likely be extrapolated to power-law bodies, which means that the direction of shock shift cannot be changed by increasing $M_\infty \tau$ for noses such that $2/3 \leq n \leq n^* \approx 0.75$, whereas this is possible for $n \geq 0.75$. Let us point out that this special nose, $n \approx 0.75$, which undergoes no shock shift in a first approximation, is also the nose for which the displacement thickness of the boundary layer follows the same power law as the body.[6] So it seems that, under the hypothesis of weak interaction, the viscous effects are not capable of modifying the results obtained here since they can be considered as a simple increase in τ in this case. The very small variation in the shock position, in particular for noses such that $n \geq 0.75$, shows that the grids in a numerical "shock capturing" approach must be very dense for the phenomenon to be observed. This extreme sensitivity of the phenomena could explain some discrepancy between numerical results and some experimental difficulties.

To conclude, Figs. 7a–7d offer examples of stream functions for $\gamma = 1.4$. For $1 < \gamma < 2$ and $2/3 < n \leq 1$, the functions Ψ_s have qualitatively the same aspect as those presented in Fig. 7a. The function Φ can be interpreted as the trace, at $x = \text{const}$, of the stream surfaces, which are meridian planes outside of the shock. Figure 7c and 7d compare the stream surfaces Φ for the cone at two different Mach numbers. The effect of the Mach number on the thickness of the shock layer is obvious; moreover, the shift of the shock position for $\alpha > 0$ can easily be observed. For $\gamma = 1.2$ the only difference with the cases presented in Figs. 7a–7d is a thinner shock layer. This flow structure stems from the appearance of a radial and a longitudinal component of the vorticity in the meridian plane. These components are of the order of α / R_x, as is the disturbance of the third component normal to the meridian plane.

Tables 1–3 give solutions for $\gamma = 1.4$ for the three noses treated earlier. A broader set of solutions is given by Andriamanalina.[13] Figure 8 gives an example of the distributions of the local quantities obtained this way. Let us point our, however, that this theory does not yield good values for ρ if $M_\infty \tau$ is not at least of the order of 10, though this does not affect the results concerning the effect of α.[11]

VII. Conclusion

Since the work presented here is the first phase of more ambitious research, the conclusion of this paper will merely point out how we will use the present results in the next stages of our approach.

At first, our analytical solutions will be compared with specific experimental tests on three slender power-law bodies at $M_\infty = 10$. The thickness ratio τ is equal to 0.4 for the three values of the power-law exponent $n = 0.67$, $n = 0.75$, and $n = 1$. The wind tunnel has been chosen to insure laminar weak interaction and no real gas effect. Measurements of pressure on the bodies and forces will be performed for $\alpha \leq 0.1$. The shock position will be obtained by different visualization techniques such as shadowgraphs, Schlieren, and differential strioinferometry. This last technique allows the quantitative measurement of the density field in the shock layer.[17] These tests are soon to be performed.

Differences or analogies between experiments and theory will give a correct evaluation of the accuracy of our hypotheses. For example, we will be able to evaluate the downstream effect of the blunted nose in the case $n = 0.75$ since the weak viscous interaction reduces to a small increase of τ but does not change the power law of the effective body. Consequently, if differences appear between experiment and theory, they have to be caused by the bluntness effect.

In a second phase, if our theoretical solution and the experiments are sufficiently close, the results of different numerical methods for the Euler equations will be compared with the theoretical field. Since the stream functions problem has been solved analytically, which is not very common for three-dimensional flows, our theory allows comparison with theoretical stream lines.

Apart from these comparisons, our research continues in two main directions. For one part, an extension of this theory for the three-dimensional boundary-layer equations is to be achieved.[18] The other way is the use of our solutions for new wave-riders design. Actually, a straightforward means to create a wave rider from one of our solutions is to use a surface $\Phi = \theta_i \approx 45$ deg for the wing and build an air intake with two symmetrical $\Phi = \theta_i \approx 160$-deg surfaces and one iso-Ψ. Figures 7a–7d give a good idea of such possibilities. But, since the flow surfaces depend on α and M_∞, the shape of the airplane will only be adapted to particular flight conditions. In Figs. 7a–7d, it can be noticed also that the sign of the curvature of the iso-Φ surfaces depends on n. So, if $\Phi = \theta_i = 45$ deg is chosen for the wing, its shape will be different for the conical wave rider ($n = 1$) and the more blunted one ($n = 0.7$).

Nevertheless, these further developments of the theory are linked to the demonstration of the accuracy of our theoretical results with the experiments.

Acknowledgment

This work has been supported by the French Ministry of Defence (DRET Groupe 6).

References

[1]Cheng, H. K, "Hypersonic Flows Past a Yawed Circular Cone and Other Bodies," *Journal of Fluid Mechanics,* Vol. 12, Pt. 2, 1962, pp. 169–191.

[2]Doty, R. T., and Rasmussen, M. L., "Approximation for Hypersonic Flow Past an Inclined Cone," *AIAA Journal,* Vol. 11, No. 6, 1973, pp. 1310–1315.

[3]Chernyi, G. G., "Application of the Equivalent Principle," *Introduction to Hypersonic Flow,* Academic, New York, 1961, pp. 82–94.

[4]Mirels, H., "Hypersonic Flow over Slender Bodies Associated with Power-Law Shocks," *Advance in Applied Mechanics,* Vol. 7, Academic, New York, 1962, pp. 1–54.

[5]Guiraud, J. P., Vallée, D., and Zolver, R., "Bluntness Effects in Hypersonic Small Disturbance Theory," *Basic Development in Fluid Dynamics,* Vol. 1, edited by M. Holt, Academic, New York, 1965, pp. 127, 247.

[6]Kubota, T., "Investigation of Flow Around Simple Bodies in Hypersonic Flow," Memorandum No. 40, Guggenheim Aeronautical Lab., California Institute of Technology, Pasadena, CA, June 1957.

[7]Lees, L., "Laminar Heat Transfer over Blunt-Nosed Bodies at Hypersonic Flight Speeds," *Jet Propulsion,* Vol. 26, No. 4, 1956, pp. 259–269.

[8]Yasuhara, M., "On the Hypersonic Viscous Flow Past Slender Bodies of Revolution," *Journal of the Physical Society of Japan,* Vol. 11, No. 8, 1956, pp. 878–886.

[9]Hayes, W. D., and Probstein, R. F., "Application of Similar Solutions to Steady Flows," *Hypersonic Flow Theory,* Vol. 1, Academic, New York, 1966, pp. 74–85.

[10]Townsend, J. C., "Second-Order Small-Disturbance Solutions for Hypersonic Flow over Power-Law Bodies," NASA TN D-7973, Nov. 1975.

[11]Merlen, A., "Un modèle analytique d'écoulement autour d'ogives élancées peu émoussées à Mach hypersonique modéré et à faible incidence," ONERA-IMFL Rept. 90/10, April 1990.

[12]Merlen, A., "Theory of Slightly Blunted Power Law Bodies at Small Angle of Attack in Hypersonic Flow," *Comptes Rendus à l'Académie des Sciences—Paris,* Vol. 310, Série II, Jan. 1990, pp. 465–470.

[13]Andriamanalina, D., "Explosion violente d'un fil rectiligne dans un écoulement, Application à l'hypersonique," Doctoral Thesis, Université des Sciences et Techniques de Lille Flandres Artois, Nov. 1990.

[14]Merlen, A., and Dyment, A., "A Theory of Anisotropic Blast Waves with Application to the Explosions in a Moving Gas," *European Journal of Mechanics, B/Fluids,* Vol. II, No. 2, 1992, pp. 761–798.

[15]Sedov, L., "Algebraic Integrals for Self-Similar Motions," *Similarity and Dimensional Methods in Mechanics*, Academic, New York, 1972, pp. 166–168.

[16]Sakuraï, A., *Blast Wave Theory: Basic Developments in Fluid Dynamic,* Vol. 1, Academic, New York, 1965.

[17]Desse, J. M., "Instantaneous Density Measurement in Two-Dimensional Gas Flow by High Speed Differential Interferometry," *Experiments in Fluids,* Vol. 9, No. 1/2, 1990, pp. 85–91.

[18]Merlen, A., Debrwyne, M. Fabre, E., and Desse, J. M., "Ecoulements Hypersoniques, Modélisation et Perspectives Expérimentales," ONERA/IMFL Rept. 91/35, Nov. 1991.